*Int. J. Electrochem. Sci.*, 10 **(2015)** 786 - 794

International Journal of
ELECTROCHEMICAL
SCIENCE
www.electrochemsci.org

# Electrodeposition of Pt-P Nanoparticles for the Electrocatalytic Oxidation of Ethanol

*Lei Shang, Faqiong Zhao, Baizhao Zeng*[*]

College of Chemistry and Molecular Sciences, Wuhan University, Wuhan, Hubei Province 430072, People's Republic of China
[*]E-mail: bzzeng@whu.edu.cn

*Received:* 21 October 2014 / *Accepted:* 27 November 2014 / *Published:* 2 December 2014

Platinum-phosphorus (Pt-P) nanoparticles were electrodeposited on a glassy carbon electrode from a solution containing 0.2 M $Na_2SO_4$, 1 mM $H_2PtCl_6$ and 0.1 mM $NaH_2PO_2$. Energy dispersive X-ray spectroscopy, X-ray photoelectron spectroscopy and X-ray diffraction revealed that P and Pt formed composite and in the Pt-P nanoparticles the content of $Pt^0$ species was higher than that in Pt nanoparticles. The resulted Pt-P catalyst exhibited enhanced electrocatalytic activity and stability for ethanol oxidation compared with Pt nanoparticles. This fabrication method was green and simple with additional reducing agents and fixative process free.

**Keywords:** Electrodeposition, Pt-P nanoparticles, Ethanol, Electrocatalytic oxidation.

## 1. INTRODUCTION

Direct alcohol fuel cells (DAFCs) have attracted increasing attention as a promising potential power generator for portable electronic devices and vehicular applications [1, 2]. Although Pt electrocatalyst is well known in these full cells, Pt is expensive and resource-limited and it also has other disadvantages [3, 4]. In order to overcome Pt electrocatalysts' shortcomings, one of the most common approaches is to prepare Pt based bimetals with other metals such as Rh, Ru, Sn, Fe, Co, Ni, Cu and Mn [5-10]. Thus the consumption of Pt can be reduced. Furthermore, the electrocatalytic activity and CO tolerance of Pt catalysts can be enhanced. However, few Pt-nonmetal composites have been reported as electrocatalyst [11, 12].

Recently, phosphorus, a common metalloid element, was incorporated into Pt to enhance the electrocatalytic activity of Pt toward the oxygen reduction reaction [11, 12]. For example, Suzuki et al

[11] fabricated highly dispersed platinum-phosphorus (Pt-P) nanoparticles on carbon support by reducing platinum ions in an aqueous solution containing hypophosphite ($H_3PO_2$). The obtained Pt-P catalyst showed higher activity to oxygen-reduction than pure Pt catalyst. Ma et al [12] prepared a carbon supported Pt-P (Pt-P/C) catalyst from $Pt(NO_3)_2$ and phosphorus yellow at room temperature. The P was thought to improve the electrocatalytic performance of Pt/C catalyst for the oxygen reduction reaction. However, to the best of our knowledge, the Pt-P catalysts have not been used for the electrochemical oxidation of ethanol. In addition, the reported preparation methods for Pt-P catalysts were complicated and time-consuming [11, 12]. Electrodeposition is a simple and controllable technique [13]; however it has not been used for the preparation of Pt-P catalyst.

In this paper, Pt-P nanoparticles are electrodeposited on a bare glassy carbon electrode (GCE). The structure and electrochemical property of the resulting Pt-P catalyst are studied by scanning electron microscopy (SEM), energy dispersive X-ray spectroscopy (EDX), X-ray photoelectron spectroscopy (XPS), X-ray diffraction (XRD) and voltammetry. The obtained Pt-P catalyst shows higher electrocatalytic activity and stability toward ethanol oxidation in comparison with the counterparting Pt nanoparticles.

## 2. EXPERIMENTAL SECTION

### *2.1 Reagents*

$H_2PtCl_6 \cdot 6H_2O$, $NaH_2PO_2 \cdot H_2O$, $H_2SO_4$, $CH_3CH_2OH$, $CuSO_4 \cdot 5H_2O$, $RuCl_3$, $NiSO_4 \cdot 6H_2O$, $NaWO_4 \cdot 2H_2O$ and $Na_2SO_4$ were purchased from Sinopharm Chemical Reagent Co. Ltd. (Shanghai, China). All chemicals used were of analytical reagent grade. The water used was redistilled.

### *2.2 Apparatus*

Electrodeposition, cyclic voltammetric (CV) and chronoamperometric experiments were performed with a CHI 604D electrochemical workstation (CH Instrument Company, Shanghai, China) and a conventional three-electrode system. The working electrode was a modified GCE (diameter: 3 mm) or a glass substrate (10 mm×10 mm×2.2 mm) coated with an indium tin oxide (ITO), and the auxiliary and reference electrodes were a platinum wire and a saturated calomel electrode (SCE), respectively. The SEM images and EDX spectroscopy were obtained by using a Hitachi X-650 SEM (Hitachi Co., Japan). XRD data were recorded with a Bruke D8 diffractometer (Germany) using Cu Kα radiation (40 kV, 40 mA) with a Ni filter. XPS was performed on an XSAM800 spectrometer (KRATOS Co., UK), using Mg Kα radiation (1253.6 eV, 16 mA × 12 kV) at a pressure of $6\times10^{-7}$ Pa. The peak positions were internally referenced to the C 1s peak at 284.6 eV. All measurements were conducted at room temperature.

*2.3 Preparation of modified electrodes and electrochemical measurements*

Pt-P catalyst was electrodeposited on a just polished GCE from a solution containing 1 mM $H_2PtCl_6$, 0.1 mM $NaH_2PO_2$ and 0.2 M $Na_2SO_4$ at room temperature. The potential was fixed at -0.3 V for 300 s. Then the resulting modified electrode (Pt-P/GCE) was washed carefully with redistilled water. For comparison, Pt/GCE was prepared by the similar method. Prior to each experiment, the working electrode was subject to potential cycling between -0.2 V and 1.2 V in 0.1 M $HClO_4$ deoxygenized by $N_2$ until a stable CV curve was obtained. Then 0.1 M ethanol was added into the solution and the CV curves for the ethanol electro-oxidation were recorded at rate of 50 mV/s.

## 3. RESULTS AND DISCUSSION

*3.1 Morphological and structure analysis*

Fig. 1 shows the SEM images of Pt and Pt-P catalysts. As can be seen, the electrodeposited Pt particles are not uniform, displaying an inhomogeneous size distribution ranging from 60 nm to 250 nm. However, the Pt-P particles are uniform, the particle diameter is about 100 nm and the particle density is higher. This indicates that $NaH_2PO_2$ is effective for reducing the size of Pt nanoparticles, promoting the deposition of Pt. This phenomenon is in line with the previous reports [11, 12].

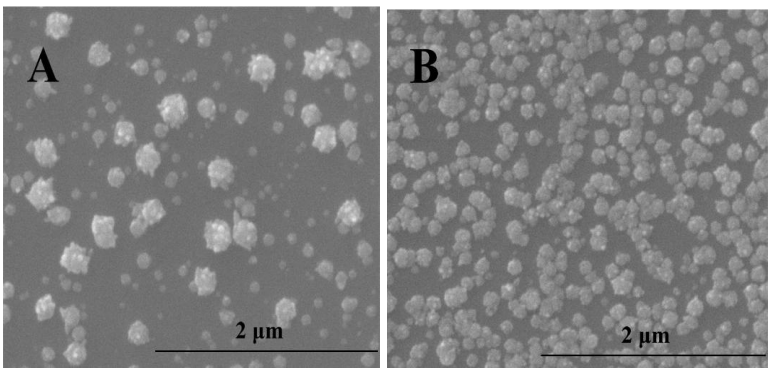


**Figure 1.** SEM images of Pt (A) and Pt-P (B) deposited. The solution for electrodeposition: 0.2 M $Na_2SO_4$ containing 1 mM $H_2PtCl_6$ (A) and 0.1 mM $NaH_2PO_2$ (B); electrodeposition potential: -0.3 V; electrodeposition time: 300 s.

In order to explore the structure of the catalyst, XRD analysis is conducted. As can be seen in Fig. 2, three peaks occur around 39.8°, 46.6° and 67.8°, respectively. According to JCPDS card 04-0784, these peaks can be assigned to Pt (111), (200) and (220), respectively. This indicates that the nanoparticles possess the face centered cubic crystal structure. The peak at 43.8° is produced by the substrate indium tin oxide. It is clear that the width of peak (111) for Pt-P catalyst is larger than that of Pt catalyst, so the average crystalline size of Pt-P nanoparticles is smaller according to the Debye-Scherrer equation [14]. This means that the incorporation of P benefits the formation of small Pt

nanoparticles. The EDX of Pt-P particles are recorded and the peaks of Pt and P are observed, meaning that Pt and P are co-deposited on the electrode. The atom ratio of Pt to P is calculated to be 5.5:1.

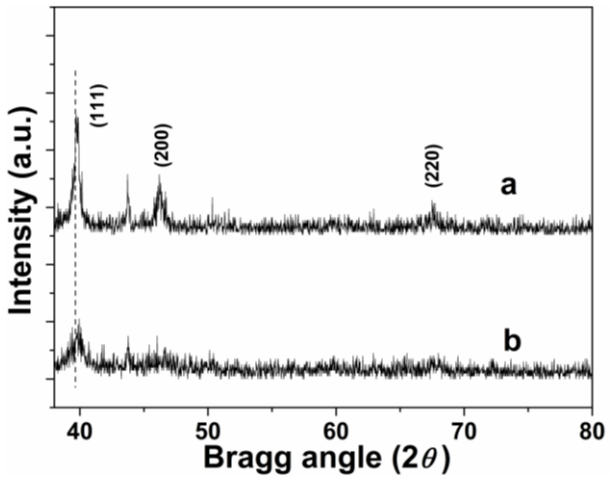


**Figure 2.** XRD patterns of Pt (a) and Pt-P (b) nanoparticles.

The structure of Pt-P composites were also characterized by XPS (Fig. 3). The presence of Pt was confirmed by the Pt $4f_{5/2}$ and $4f_{7/2}$ regions at binding energies of about 74.6 eV and 71.4 eV (Fig. 3A), respectively [15, 16]. A binding energy of 133.8 eV is also observed (Fig. 3B), assigned to oxidized phosphorus ($P^{v}$) [17, 18]. The result indicates that most P in the Pt-P catalyst is at the oxide state.

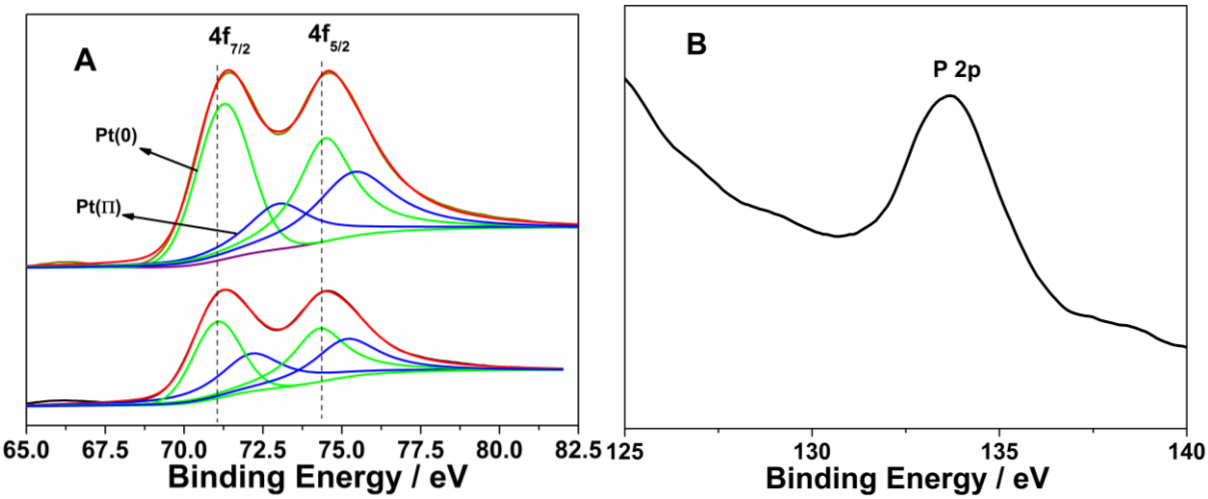


**Figure 3.** (A) XPS spectra of Pt 4f for Pt-P catalyst (upper) and Pt catalyst (bottom). (B) XPS spectra of P 2p for Pt-P catalyst.

The atom ratio of Pt to P is estimated to be 5.4:1, which is in line with the result of EDS analysis. In addition, each Pt 4f peak of Pt-P catalyst can be fitted to two pairs of doublets. Pt $4f_{7/2}$ peak

at 71.27 eV and Pt $4f_{5/2}$ peak at 74.47 eV are assigned to $Pt^0$, while Pt $4f_{7/2}$ peak at 73.02 eV and Pt $4f_{5/2}$ peak at 75.39 eV belong to $Pt^{II}$ [12]. Compared with Pt nanoparticles, the binding energy values of $Pt^0$ and $Pt^{II}$ in Pt-P nanoparticles shift positively a little, attributed to strong Pt-P interaction. The reason is that when Pt interacts with P it would donate electrons to P, causing the decrease of the 4f electron density of Pt. Moreover, the area ratio of $Pt^0$ peak to $Pt^{II}$ peak in Pt-P nanoparticles is higher than that in Pt nanoparticles, indicating that the introduction of P can make the relative content of $Pt^0$ significantly increase. This can be explained as follows: the $Pt^{II}$ peaks may be produced by the Pt-$O_{ad}$ bonds at the surface layer [19, 20]. When P is doped into Pt, the oxidized phosphorus species on Pt nanoparticle surface restrains the interaction between Pt atom and $O_2$ in air [21], thus the formation of Pt-$O_{ad}$ bonds is restricted.

### *3.2 Electrocatalytic performance of Pt-P catalysts*

To study the electrochemical properties of the catalysts, CV curves of Pt and Pt-P nanoparticles are recorded in a $N_2$ saturated 0.1 M $HClO_4$ solution (Fig. 4A). As well known, the electrochemically active surface area (ECSA) of Pt nanoparticles can be estimated from the integrated charge in the hydrogen adsorption/desorption region of the cyclic voltammogram according to the following equation [22]:

$$A=Q_H / 0.21 \text{ mC cm}^{-2}$$

Where $A$ represents the ECSA of the Pt nanoparticles, $Q_H$ is the amount of charge corresponding to the hydrogen adsorption/desorption region, and 0.21 mC $cm^{-2}$ is the charge density of Pt with a monolayer adsorption of hydrogen. The ECSA represents the number of Pt sites that are available for hydrogen adsorption and desorption. It can be observed that the Pt-P catalyst presents larger hydrogen adsorption/desorption peaks than the Pt catalyst, reflecting the larger electrochemically active surface area of Pt-P catalyst.

The electrocatalytic properties of the two catalysts toward ethanol oxidation are compared in Fig. 4B. Their voltammograms are similar, two anodic peaks are observed for the anodic scan, and one peak for the cathodic scan. The first peak for ethanol oxidation can be explained by a two-path mechanism, with the formation of $CO_{ads}$ strongly bonded to the Pt surface and the oxidation of Pt particles [23, 24]. The–second peak is related to the production of $CO_2$ and carboxylic acid and the peak for the backward scan is related to the re-oxidation of adsorbed ethanol [23, 24]. When the peak current densities are normalized to the ECSA of the catalysts (Fig. 4B) they are 1.15 and 0.90 mA $cm^{-2}$ for Pt-P catalyst, which are 1.5 times as big as those for the Pt catalyst. Meanwhile, the onset oxidation potential is slightly lower, illustrating that the Pt-P nanoparticles have higher electrocatalytic activity towards the ethanol. In addition, the peak current ratio of the forward to backward scans ($I_f/I_b$) for ethanol electrooxidation at Pt-P catalyst is higher than that at Pt catalyst, reflecting the higher poisoning tolerance of Pt-P catalyst [25, 26]. The enhanced electrocatalytic activity of Pt-P catalyst can be ascribed to the synergistic effect between Pt and P. The incorporated P lowers the Fermi level in the 5d Pt band and makes the bond energy between Pt and $CO_{ads}$ decrease [27-30]. Such bond energy reduction improves the poisoning tolerance of Pt-P catalyst during the ethanol electrooxidation.

The stability of the catalyst is studied by chronoamperometry. As demonstrated in Fig. 4C, a decrease in the current density is observed for both catalysts with time going, which could be attributed to the intermediated poisoning species formed during the electrooxidation of ethanol. Noticeably, the Pt-P catalyst shows higher initial current density and limiting current density for a long time. This indicates that the Pt-P catalyst has higher electroactivity and stability than Pt catalyst for ethanol electrooxidation.

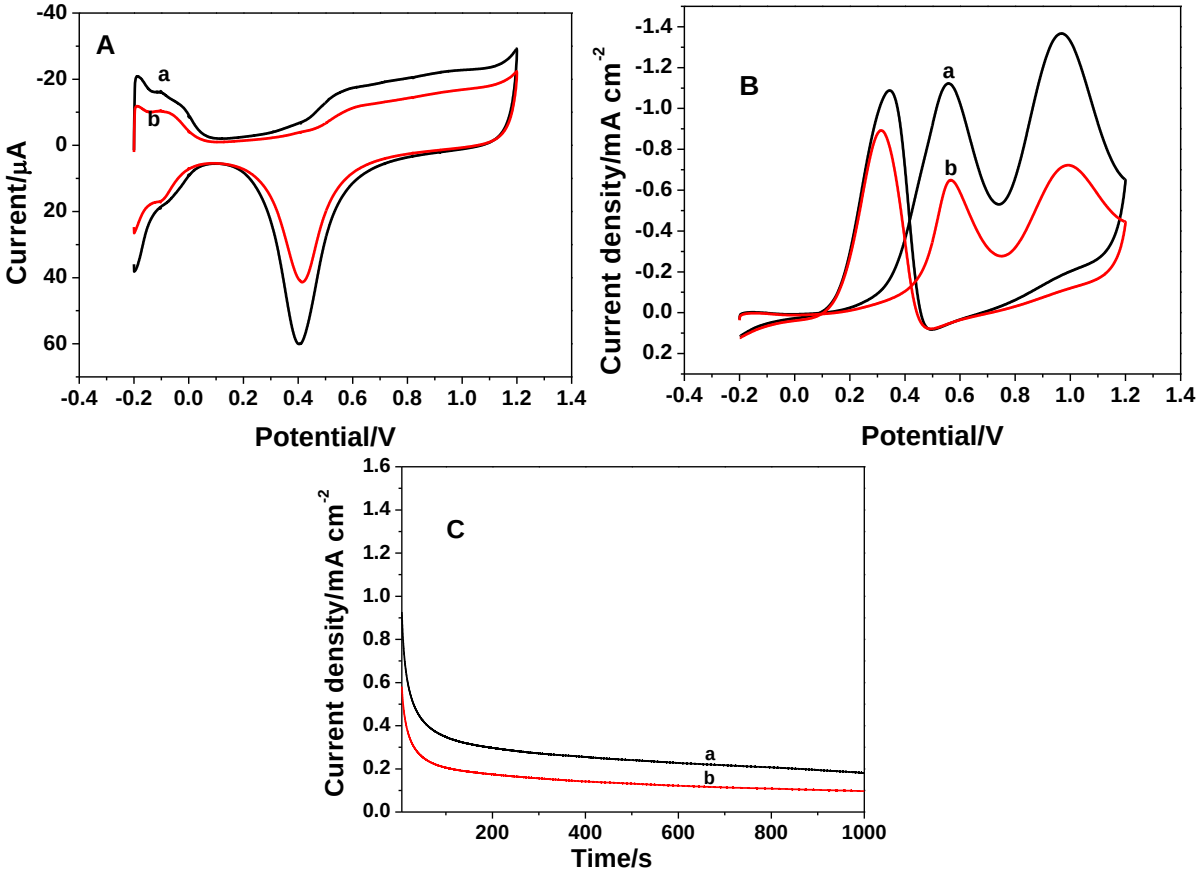


**Figure 4.** (A) Cyclic voltammograms of Pt-P (a) and Pt (b) catalysts in 0.1 M $HClO_4$ solution at 50 mV $s^{-1}$. (B) Cyclic voltammograms of Pt-P (a) and Pt (b) catalysts in 0.1 M $HClO_4$ + 0.1 M $CH_3CH_2OH$ solution at 50 mV $s^{-1}$. (C) Chronoamperometric curves of Pt-P (a) and Pt (b) catalysts in 0.1 M $HClO_4$ + 0.1 M $CH_3CH_2OH$ solution at 0.6 V.

### *3.3 The effect of the third element*

Since some metals such as Ni [7] and Ru [10] can also enhance the electrocatalytic activity and CO tolerance of Pt catalyst, the influence of several elements (i.e. Ru, Ni, W and Cu) on the catalytic activity of Pt-P catalyst is tested. Among the obtained catalysts the Pt-Ru-P catalyst is prepared by electrodeposition in a solution containing 1 mM $H_2PtCl_6$, 0.1 mM $NaH_2PO_2$, 0.5 mM $RuCl_3$ and 0.2 M $Na_2SO_4$ at -0.3 V for 300 s; the Pt-Cu-P catalyst is prepared by the same way except replacing 0.5 mM $RuCl_3$ with 0.5 mM $CuSO_4$. Pt-Ni-P and Pt-W-P are obtained through electrodepositing at -0.6 V for

300 s in a solution containing 1 mM $H_2PtCl_6$, 0.1 mM $NaH_2PO_2$, 50 mM $NiSO_4$ (or 5 mM $Na_2WO_4$) and 0.2 M $Na_2SO_4$. Fig. 5 shows the cyclic voltammograms of five different catalysts in ethanol solution. The anodic peak current densities corresponding to the forward scan of Pt-Ru-P, Pt-Cu-P and Pt-Ni-P are 1.4, 1.3 and 1.15 times as high as that of Pt-P catalyst, respectively, meaning that there is synergistic effect between the third element and Pt-P. However, when W is doped into Pt-P catalyst the peak current density decreases. This is related to the poor catalytic activity of W. Therefore, the catalytic property of Pt-P catalyst can still be improved by introducing other component.

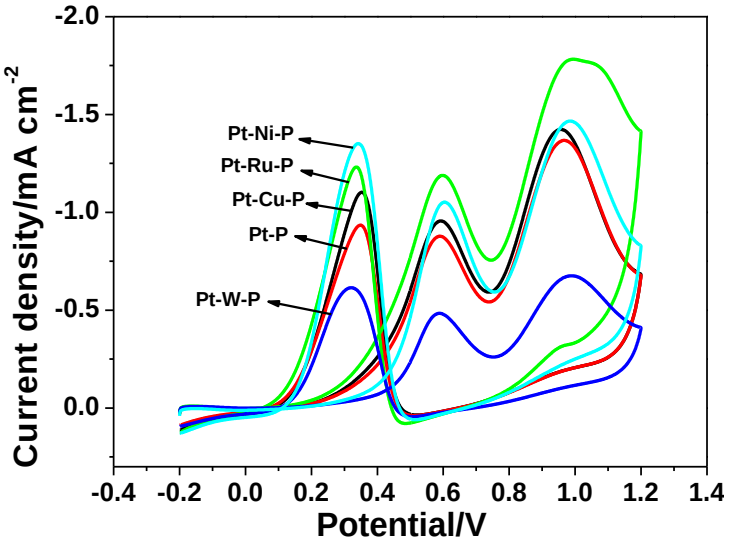


**Figure 5.** Cyclic voltammograms of Pt-W-P, Pt-P, Pt-Cu-P, Pt-Ni-P and Pt-Ru-P catalysts (from inner to outer) in 0.1 M $HClO_4$ + 0.1 M $CH_3CH_2OH$ solution at 50 mV $s^{-1}$.

## 4. CONCLUSIONS

In this work, a Pt-P catalyst was successfully prepared by co-deposition of Pt and P on a bare GCE at room temperature. The obtained catalyst exhibited enhanced catalytic activity and stability towards the electrooxidation of ethanol in comparison with the corresponding Pt nanoparticles. The preparation method is simple, green and has promising applications in full cells. In addition, the electrocatalytic activity of Pt-P catalyst can be improved by introducing other component.

ACKNOWLEDGEMENTS
The Authors appreciate the financial support of the National Natural Science Foundation of China (Grant No.: 21075092 ) and the State Key Laboratory of Advanced Technology for Materials Synthesis and Processing (Wuhan University of Technology, Grant No. 2010-KF-12).

*Supplementary Materials:*

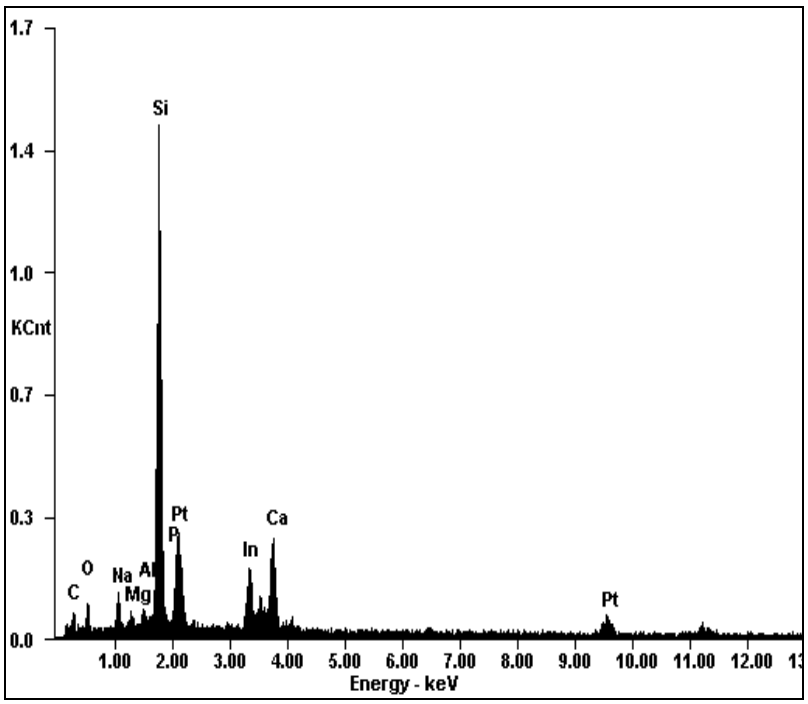


**Figure S1** EDS spectrum of the Pd–P nanoparticles.

## References

1. E. Reddington, A. Sapienza, B. Gurau, R. Viseanathan, S. Sarangapani, E.S. Smotkin, T.E. Mallout, *Science*, 280 (1998) 1735-1736.
2. K.W. Park, J.H. Choi, B.K. Kwon, S.A. Lee, Y.E. Sung, H.Y. Ha, S.A. Hong, H. Kim, A. Wieckowski, *J. Phys. Chem. B*, 106 (2002) 1869-1877.
3. J.M. Leger, S. Rousseau, C. Coutanceau, F. Hahn, C. Lamy, *Electrochim. Acta*, 5 (2005) 5118-5125.
4. H. Wang, Z. Jusys, R.J. Behm, *J. Phys. Chem. B*, 108, (2004) 19413-19424.
5. J.P.I. de Souza, S.L. Queiroz, K. Bergamaski, E.R. Gonzalez, F.C. Nart, *J. Phys. Chem. B*, 10 (2002) 9825-9830.
6. L.H. Jiang, G.Q. Sun, S.G. Sun, J.G. Liu, S.H. Tang, H.Q. Li, B. Zhou, Q. Xin, *Electrochim. Acta*, 50 (2005) 5384-5389.
7. C.T. Hsieh, J.Y. Lin, *J. Power Sources*, 188 (2009) 347-352.
8. R. Srivastava, P. Mani, N. Hahn, P. Strasser, *Angew. Chem. Int. Ed.*, 46 (2007) 8988-8994.
9. Y.J. Kang, C.B. Murray, *J. Am. Chem. Soc.*, 132 (2010) 7568-7569.
10. H. Wang, Z. Jusys, R.J. Behm, *J. Power Sources*, 154 (2006) 351-359.
11. S. Suzuki, Y. Ohbu, T. Mizukami, Y. Takamori, M. Morishima, H. Daimon, M. Hiratani, *J. Electrochem. Soc.*, 156 (2009) B27-B31.
12. J.A. Ma, Y.W. Tang, G.X. Yang, Y. Chen, Q. Zhou, T.H. Lu, J.W. Zheng, *Appl. Surf. Sci.*, 257 (2011) 6494-6497.
13. B.M. Quinn, C. Dekker, S.G. Lemay, *J. Am. Chem. Soc.*, 127 (2005) 6146-6147.
14. V. Ponec, G.C. Bond, *Catalysis by Metals and Alloy*s, Elsevier, Amsterdam (1995).
15. G.J. Wang, Y.Z. Gao, Z.B. Wang, C.Y. Du, J.J. Wang, G.P. Yin, *J. Power Sources*, 195 (2010) 185-189.

16. Z.B. Wang, P.J. Zuo, G.J. Wang, C.Y. Du, G.P. Yin, *J. Phys. Chem. C*, 112 (2008) 6582-6587.
17. G. Yang, Y. Chen, Y. Zhou, Y. Tang, T. Lu, *Electrochem. Commun.*, 12 (2010) 492-495.
18. H.B. Lee, D.S. Wuu, C.Y. Lee, C.S. Lin, *Metal. Mater. Trans. A*, 41 (2009) 450-455.
19. J.H. Kim, S.M. Choi, S.H. Nam, M.H. Seo, S.H. Choi, W.B. Kim, *Appl. Catal., B*, 82 (2008) 89-102.
20. G. Neri, C. Milone, S. Galvagno, A.P.J. Pijpers, J. Schwank, *Appl. Catal., A*, 227 (2002) 105-110.
21. H.J. Sun, J.F. Xu, G.T. Fu, X.B. Mao, L. Zhang, Y. Chen, Y.M. Zhou, T.H. Lu, Y.W. Tang, *Electrochim. Acta*, 59 (2012 ) 279-283.
22. Z. Liu, J.Y. Lee, W. Chen, M. Han, L.M. Gan, *Langmuir*, 20 (2004) 181-187.
23. S. Chen, M. Schell, *J. Electroanal. Chem.*, 478 (1999) 108-117.
24. R.T.S. Oliveira, M.C. Santos, B.G. Marcussi, S.T. Tanimoto, L.O.S. Bulhoes, E.C. Pereira, *J. Power Sources*, 157 (2006) 212-216.
25. L.F. Dong, R.R.S. Gari, Z. Li, M.M. Craig, S.F. Hou, *Carbon*, 48 (2010) 781-787.
26. J.M. Sieben, M.M.E. Duarte, *Int. J. Hydrogen Energy*, 37 (2012) 9941-9947.
27. K. Zhang, Q. Yue, G. Chen, Y. Zhai, L. Wang, H. Wang, J. Zhao, J. Liu, J. Jia, H. Li, *J. Phys. Chem. C*, 115 (2011) 379-389.
28. M. Wakisaka, S. Mitsui, Y. Hirose, K. Kawashima, H. Uchida, M. Watanabe, *J. Phys. Chem. B*, 110 (2006) 23489-23496.
29. A.K. Shukla, M. Neergat, P. Bera, V. Jayaram, M.S. Hegde, *J. Electroanal. Chem.*, 504 (2001) 111-119.
30. S. Lee, H.J. Kim, S.M. Choi, M.H. Seo, W.B. Kim, *Appl. Catal., A*, 429 (2012) 39-47.`